

# The Role of Fin Geometry in Heat Sink Performance

**W. A. Khan**

Department of Mathematics,  
COMSATS Information Technology Center,  
University Road, 22060,  
NWFP, Pakistan

**J. R. Culham**

**M. M. Yovanovich**

Microelectronics Heat Transfer Laboratory,  
Department of Mechanical Engineering,  
University of Waterloo,  
Waterloo, Ontario N2L 3G1,  
Canada

*The following study will examine the effect on overall thermal/fluid performance associated with different fin geometries, including, rectangular plate fins as well as square, circular, and elliptical pin fins. The use of entropy generation minimization, EGM, allows the combined effect of thermal resistance and pressure drop to be assessed through the simultaneous interaction with the heat sink. A general dimensionless expression for the entropy generation rate is obtained by considering a control volume around the pin fin including base plate and applying the conservations equations for mass and energy with the entropy balance. The formulation for the dimensionless entropy generation rate is developed in terms of dimensionless variables, including the aspect ratio, Reynolds number, Nusselt number, and the drag coefficient. Selected fin geometries are examined for the heat transfer, fluid friction, and the minimum entropy generation rate corresponding to different parameters including axis ratio, aspect ratio, and Reynolds number. The results clearly indicate that the preferred fin profile is very dependent on these parameters.*

[DOI: 10.1115/1.2351896]

## Introduction

While heat sinks are routinely used in most electronics applications, the rationale for selecting a particular design of heat sink or more specifically a particular fin cross sectional profile, remains somewhat uncertain. Most often these types of selection procedures are based exclusively on performance evaluations consisting of formulations for extended surface heat transfer found in most fundamental heat transfer text books. Unfortunately, these formulations do not consider the role of pressure drop in determining the local fin velocity or heat transfer coefficient and, therefore, the resulting heat transfer calculations rarely pertain to actual flow conditions. The effects of viscous dissipation associated with flow past fins of arbitrary cross section can be conveniently coupled with the thermal resistance to heat flow in forced convection by using entropy generation minimization (EGM). Entropy generation minimization combines the fundamental principles of thermodynamics, heat transfer, and fluid mechanics and applies these principles to the modeling and optimization of real systems and processes that are characterized by finite size and finite time constraints, and are limited by heat and mass transfer and fluid flow irreversibilities.

A careful review of the literature reveals that no theoretical study exists which compares the overall performance of the different fin geometries (selected in this study) based on the thermal as well as the hydraulic resistance. Behnia et al. [1] compared numerically the heat transfer performance of various commonly used fin geometries (circular, square, rectangular, and elliptical). They fixed the fin cross-sectional area per unit base area, the wetted surface area per unit base area, and the flow passage area for all geometries. They found that circular pin fins outperform square pin fins and elliptical fins outperform plate fins. They also found that elliptical fins work best at lower values of pressure drop and pumping work whereas round pin fins offer highest performance at higher values. Li et al. [2] showed experimentally that the heat transfer rate with elliptical pin fins is higher than that with circular pin fins while the resistance of the former is much lower than that of the latter in the Reynolds number range from 1000 to 10,000. Chapman et al. [3] investigated experimentally the paral-

lel plate fins and cross-cut pin fins in low air flow environments and compared these fins with elliptical pin fin heat sinks. They used equal volume heat sinks in their experiments. They found that the overall thermal resistance of the parallel plate fin was lower than the other two designs, whereas the heat transfer coefficient was highest for elliptical pin fins. Ota et al. [4,5] studied experimentally heat transfer and flow around an elliptical cylinder of axes ratios 1:2 and 1:3. Their experimental results show that heat transfer coefficient of the elliptical cylinder is higher than that of a circular one with equal circumference and the pressure drag coefficients of the former are much lower than that of the later. Poulidakos and Bejan [6] established a theoretical framework to determine the optimum fin dimensions for minimum entropy generation in forced convection. They first developed an expression for the entropy generation rate for a general fin and then applied it to select the optimum dimensions of pin fins, rectangular plate fins, plate fins with trapezoidal cross section, and triangular plate fins with rectangular cross section. Their study seems to be inconclusive as to which geometry offers advantages over others. Jonsson and Bjorn [7] performed experiments to compare the thermal performance of the heat sinks with different fin designs including straight fins and pin fins with circular, quadratic, and elliptical cross sections. They evaluated the thermal performance by comparing the thermal resistance of the heat sinks at equal average velocity and equal pressure drop. They recommended elliptical pin-fins at high velocities and circular pin-fins at mid-range velocities. Wirtz et al. [8] reported experimental results on the thermal performance of model pin-fin fan-sink assemblies. They used cylindrical, square, and diamond shape cross section pin-fins and found that cylindrical pin-fins give the best overall fan-sink performance. Furthermore, the overall heat sink thermal resistance decreases with an increase in either applied pressure rise or fan power and fin height. Laor and Kalman [9] investigated the performance of longitudinal fins, spines, and annular fins having rectangular, triangular, and parabolic shapes with uniform and nonuniform heat generation and temperature distributions, whereas Mokheimer and Esmail [10] investigated the performance of annular fins of different profiles subject to locally variable heat transfer coefficient.

Culham and Muzychka [11] presented a method to optimize plate fin heat sink based on the minimization of entropy generation resulting from viscous fluid effects and heat transfer. They used a novel approach for incorporating forced convection

Contributed by the Electronic and Photonic Packaging Division of ASME for publication in the JOURNAL OF ELECTRONIC PACKAGING. Manuscript received July 13, 2004; final manuscript received February 24, 2006. Review conducted by Koneru Ramakrishna.

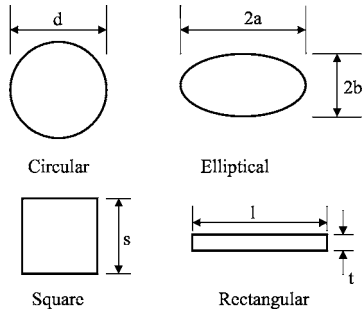


Fig. 1 Cross sections of selected geometries

through the specification of a fan curve into the optimization procedure, providing a link between optimized design parameters and the system operating point. Bar-Cohen and his co-workers [12–15] performed a least material optimization of plate-fin geometry by extending the use of least-material single fin analysis to multiple fin arrays. They explored the potential for the least-energy optimization of natural and forced convection cooled rectangular plate heat sinks. The results are evaluated in terms of a heat sink coefficient of performance, relating the cooling capability to the energy invested in the fabrication and operation of the heat sink, and compared to the entropy generation minimization methodology (EGM).

This study will show in a graphical manner the relationship between the dimensionless entropy generation rate and the parameters including Reynolds number, aspect ratio and axis ratio. The results will allow designers to quickly and easily assess the merits of pin fin geometries for specific design conditions.

### Assumptions

This study is based on the following assumptions:

- (1) The fin material is homogeneous and isotropic;
- (2) the flow is steady, laminar and two dimensional;
- (3) the fluid is considered incompressible with constant properties;
- (4) the heat transfer coefficient is uniform over the fin surface;
- (5) there is no contact resistance between fin and the baseplate;
- (6) there are no heat sources within the fin itself;
- (7) there is no free convection or radiation heat transfer.

### Analysis

Consider a fin of arbitrary cross section (rectangular, circular, square, or elliptical as shown in Fig. 1), which is extended from a base plate. The approach velocity of the air is  $U_{app}$  and the ambient temperature of the air is assumed to be  $T_a$ . The surface temperature of the pin wall is  $T_w (> T_a)$ .

The entropy generation model can be developed by following Bejan [16] and considering the control volume CV as shown in Fig. 2. This control volume includes a pin-fin and a baseplate. The side surfaces AEFB and BCJI and the top surface CJFE of this CV can be regarded as impermeable, adiabatic and shear free (no mass transfer and shear work transfer across these surfaces). The heat transferred from the base plate in the CV is  $Q$ . The bulk properties of air are represented by  $u_{in}, P_{in}, s_{in}$  at the inlet and by  $u_{out}, P_{out}, s_{out}$  at the outlet respectively. Fluid friction is represented by  $F_D$ , which is the sum of the friction and pressure drags. The irreversibility of this system is due to heat transfer across the nonzero temperature difference  $T_b - T_a$  and to frictional drag.

The mass rate balance for the CV, shown in Fig. 3, gives

$$\frac{dm_{cv}}{dt} = \dot{m}_{in} - \dot{m}_{out} \quad (1)$$

For steady state, it reduces to

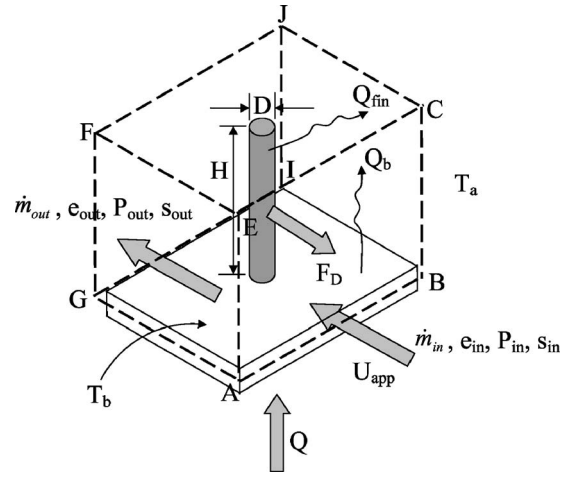


Fig. 2 Control volume for calculating  $\dot{S}_{gen}$  for single circular pin

$$\dot{m}_{in} = \dot{m}_{out} = \dot{m} \quad (2)$$

First law of thermodynamics for the same CV can be written as

$$\frac{dE_{cv}}{dt} = Q - \dot{W}_{cv} + \dot{m}_{in}(e_{in} + P_{in}v_{in}) - \dot{m}_{out}(e_{out} + P_{out}v_{out}) \quad (3)$$

where

$dE_{cv}/dt$  = time rate of change of energy within CV

$Q$  = heat transferred from base plate in CV

$\dot{W}_{cv}$  = energy transfer by work across the boundaries of CV

$e_{in}, e_{out}$  = specific energies at the inlet and exit of CV

$P_{in}, P_{out}$  = pressure at the inlet and exit of CV

$v_{in}, v_{out}$  = specific volume of fluid at the inlet and exit of CV.

For steady state,  $dE_{cv}/dt=0$ . The specific energy  $e$  is the sum of specific internal, kinetic, and potential energies. Due to continuity and same elevation of the CV,  $V_{in}=V_{out}$  and  $z_{in}=z_{out}$ , so the kinetic and potential energy terms will drop out. Therefore,  $e_{in}=u_{in}$  and  $e_{out}=u_{out}$ . The only work is flow work at the inlet and exit of the CV, so the term  $\dot{W}_{cv}$  also drops out. Thus the energy rate balance reduces to:

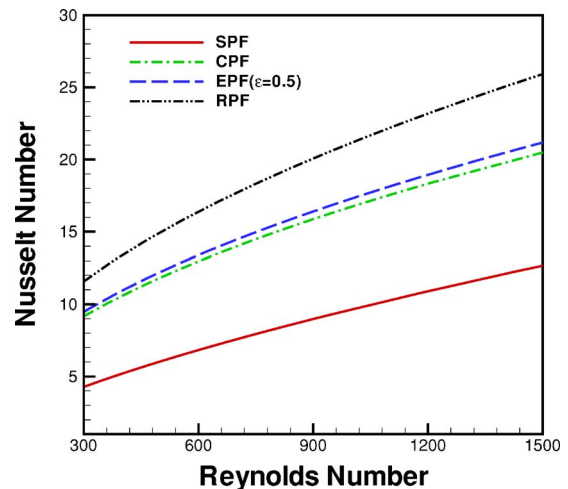


Fig. 3 Effect of the Reynolds number on heat transfer coefficients

**Table 1 Parameters for different geometries**

Parameters	Geometry				Reference
	Plate	Circular	Square	Elliptical	
$\mathcal{L}$	$l$	$d$	$s$	$2a$	
$A_c$	$tl$	$\pi d^2/4$	$s^2$	$\pi ab$	
$A_p$	$LH$	$dH$	$sH$	$2aH$	
$P$	$2(l+t)$	$\pi d$	$4s$	$4aE(e)$	
$C_1$	1.357	5.781	0	$-4.1[0.67 - \exp(0.733e)]$	[17]
$C_2$	0	1.152	2	$1.1526e^{0.951}$	[17]
$C_3$	0	1.26	0	$1.26e^{0.95}$	[17]
$C_4$	0.75	0.593	0.102	$0.75 - 0.16 \exp(-0.018e^{-3.1})$	[17]
$C_5$	$2\epsilon_1(1 + \epsilon_1)$	$\pi^2/4$	4	$\pi^4 \epsilon / 16E^2(e)$	[17]
$C_6$	$2(1 + \epsilon_1) / \epsilon_1$	4	4	$16E^2(e) / \pi^2 \epsilon$	[17]
$n$	1/2	1/2	0.675	1/2	[18]

$$Q = \dot{m} \left[ \underbrace{(u_{out} + P_{out}v_{out})}_{h_{out}} - \underbrace{(u_{in} + P_{in}v_{in})}_{h_{in}} \right] \quad (4)$$

The combination of specific internal and flow energies is defined as specific enthalpy; therefore, the energy rate balance reduces further to

$$Q = \dot{m}(h_{out} - h_{in}) \quad (5)$$

From the second law of thermodynamics

$$\frac{dS_{cv}}{dt} = \dot{m}(s_{in} - s_{out}) + \frac{Q}{T_b} + \dot{S}_{gen} \quad (6)$$

For steady state,  $dS_{cv}/dt=0$ , and the total heat transferred from the baseplate  $Q=Q_{fin}+Q_b$ , so the entropy rate balance reduces to

$$\dot{S}_{gen} = \dot{m}(s_{out} - s_{in}) - \frac{Q}{T_b} \quad (7)$$

where  $T_b$  represents the baseplate absolute temperature. From a force balance, the total drag force can be written as

$$F_D = -(P_{out} - P_{in})A \quad (8)$$

where  $A$  is the free stream cross-sectional area. The mass flow rate is given by

$$\dot{m} = \rho A U_{app} \quad (9)$$

where  $\rho$  is the density of the fluid at the ambient temperature. The enthalpy difference in Eq. (5) can be written in terms of entropy and pressure differences using Gibb's equation [ $dh = Tds + (1/\rho)dP$ ]

$$h_{out} - h_{in} = T_a(s_{out} - s_{in}) + \frac{1}{\rho}(P_{out} - P_{in}) \quad (10)$$

Combining Eqs. (2)–(10), the entropy generation rate can be written as

$$\dot{S}_{gen} = Q \left[ \frac{1}{T_a} - \frac{1}{T_b} \right] + \frac{F_D U_{app}}{T_a} \quad (11)$$

Rearranging the terms and writing  $\theta_b = T_b - T_a$ , we have

$$\dot{S}_{gen} = \frac{Q\theta_b}{T_a T_b} + \frac{F_D U_{app}}{T_a} \quad (12)$$

As  $\theta_b = QR_{tot}$ , the entropy generation rate can be written as

$$\dot{S}_{gen} = \frac{Q^2 R_{tot}}{T_a T_b} + \frac{F_D U_{app}}{T_a} \quad (13)$$

This expression describes the entropy generation rate model completely and it shows that the entropy generation rate depends on the total thermal resistance  $R_{tot}$  and the drag force, provided that the heat load and ambient conditions are specified.

The drag force is defined as

$$F_D = C_D \left( \frac{1}{2} \rho U_{app}^2 \right) A_p \quad (14)$$

where  $C_D$  is the drag coefficient and is given by Khan [17]

$$C_D = \frac{C_1}{\sqrt{Re_{\mathcal{L}}}} + C_2 + \frac{C_3}{Re_{\mathcal{L}}} \quad (15)$$

The constants  $C_1$ ,  $C_2$ , and  $C_3$  depend upon the geometry and are tabulated in Table 1.

Assuming that the thermal spreading and contact resistances are negligible, the total thermal resistance  $R_{tot}$  can be written as

$$R_{tot} = \frac{1}{\frac{1}{R_{fin}} + \frac{1}{R_{film}}} \quad (16)$$

where

$$R_{fin} = \frac{1}{\sqrt{h_{fin} P k A_c \tanh(mH)}} \quad (17)$$

$$R_{film} = \frac{1}{h_b(LW - A_c)} \quad (18)$$

with

$$m = \sqrt{\frac{h_{fin} P}{k A_c}} \quad (19)$$

$$h_{fin} = \frac{Nu_{\mathcal{L}} k_f}{\mathcal{L}} \quad (20)$$

$$h_b = \frac{Nu_L k_f}{L} \quad (21)$$

where the dimensionless average heat transfer coefficients  $Nu_{\mathcal{L}}$  for the selected geometries and  $Nu_b$  for the base plate are developed by Khan [17] and can be written as

$$Nu_{\mathcal{L}} = C_4 Re_{\mathcal{L}}^n Pr^{1/3} \quad (22)$$

$$Nu_L = 0.75 Re_b^{1/2} Pr^{1/3} \quad (23)$$

with

$$Re_{\mathcal{L}} = \frac{\mathcal{L} U_{app}}{\nu} \quad \text{and} \quad Re_L = \frac{L U_{app}}{\nu} \quad (24)$$

The constant  $C_4$  and the index  $n$  for all geometries are given in Table 1. In dimensionless form, entropy generation rate, Eq. (13), for any arbitrary cross section is written as

**Table 2** Dimensions used to determine performance of fin geometry

Quantity	Dimension
Footprint (mm <sup>2</sup> )	50 × 50
Baseplate thickness (mm)	2
Overall height of fin (mm)	12
Thickness of RPF (mm)	1
Approach velocity (m/s)	3
Thermal conductivity of solid (W/m·K)	237
Thermal conductivity of air (W/m·K)	0.026
Density of air (kg/m <sup>3</sup> )	1.1614
Specific heat of air (J/kg·K)	1007
Kinematic viscosity (m <sup>2</sup> /s)	1.58 × 10 <sup>-5</sup>
Prandtl number (Air)	0.71
Heat load (W)	10
Ambient temperature (K)	300
Base plate temperature (K)	350

$$\begin{aligned}
 N_s &= \frac{\dot{S}_{gen}}{(Q^2 U_{app} / k_f \nu T_a^2)} \\
 &= \frac{T_a k_{eq}}{T_b Re_L (\sqrt{C_5 Nu_L k_{eq}} \tanh(\gamma_L \sqrt{C_6 Nu_L k_{eq}}) + C_7 Nu_L k_{eq})} \\
 &\quad + \frac{1}{2} B Re_L^2 C_D \gamma_L \quad (25)
 \end{aligned}$$

where  $\gamma_L$  is the aspect ratio of the fin,  $k_{eq}$  is the ratio of the thermal conductivities of fluid to the fin material,  $T_a$  and  $T_b$  are the ambient and base plate temperatures,  $B$  is a fixed dimensionless duty parameter that accounts for the importance of fluid friction irreversibility relative to heat transfer irreversibility and  $C_5$ ,  $C_6$ , and  $C_7$  are the constants depending on the geometry of the fin and are given by

$$C_5 = \frac{PA_c}{L^3}$$

$$C_6 = \frac{PL}{A_c}$$

$$C_7 = \frac{W}{L} - \frac{A_c}{L^2}$$

The values of these constants for the selected geometries are also given in Table 1. The cross sections for rectangular plate fin (RPF), circular pin fin (CPF), square pin fin (SPF), and elliptical pin fin (EPF) are shown in Fig. 1 and a summary of different parameters for the selected geometries is given in Table 1.

## Results and Discussion

The quantities given in Table 2 are used as the default case to compare the overall performance of each fin geometry based on the same perimeter. The air properties are evaluated at the ambient temperature. Equation (25) shows that the dimensionless entropy generation rate depends upon the heat transfer and drag coefficients. It increases with the decrease in heat transfer and increase in the drag coefficients. These coefficients depend upon the Reynolds numbers and fluid properties. The dependence of these coefficients on the Reynolds number is shown in Figs. 3 and 4. Figure 3 shows the increase in Nusselt number with the Reynolds number. For the same perimeter of each pin fin, the heat transfer from a SPF is the least, whereas for other geometries it increases from CPF to RPF as the axis ratio of EPF decreases. From heat transfer point of view, EPF with smaller axis ratio and RPF give better thermal performance. Figure 4 shows the hydraulic performance of each pin fin. For the same perimeter of each pin fin, the drag coefficient of a SPF is the highest whereas for the RPF is the

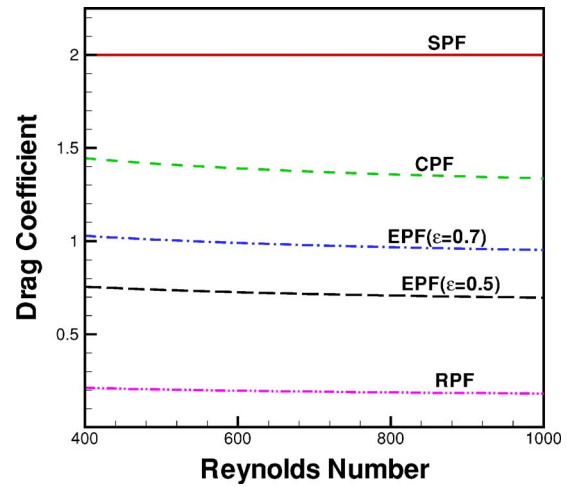


**Fig. 4** Effect of the Reynolds number on drag coefficients

least. The drag coefficient of EPF decreases from CPF to RPF as the axis ratio decreases. The dependence of drag coefficients on the Reynolds number decreases with the decrease in the axis ratio.

The dependence of heat transfer and drag coefficients on the axis ratio for EPF having the same perimeter is shown in Figs. 5 and 6 for three different approach velocities. Figure 5 shows the increase in heat transfer coefficients with the decrease in the axis ratio. These coefficients increase with the decrease in the axis ratio and the increase in approach velocities. From heat transfer point of view, EPF with a smaller axis ratio gives the best thermal performance of a heat sink. The effect of axis ratio on the drag coefficients is shown in Fig. 6 for EPF. It shows the strong dependence of axis ratio and weak dependence of approach velocity on the drag coefficients. From hydraulic point of view, EPF with smaller axis ratio gives the best performance in a heat sink.

Equation (25) also shows that the total dimensionless total entropy generation rate,  $N_s$ , is due to heat transfer and viscous friction. These contributions depend upon many parameters including perimeter and approach velocity, and show the same behavior for each geometry, i.e., the entropy generation rate due to heat transfer decreases whereas the entropy generation rate due to viscous friction increases with each parameter. This behavior is shown in Fig. 7 for a CPF. It shows that as the perimeter is increased, the contribution due to heat transfer,  $N_{sh}$ , decreases and that of viscous friction,  $N_{sf}$ , increases.

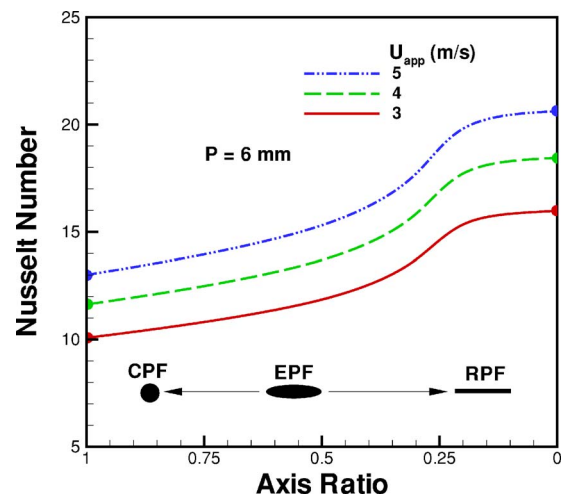


**Fig. 5** Effect of the axis ratio on heat transfer coefficients

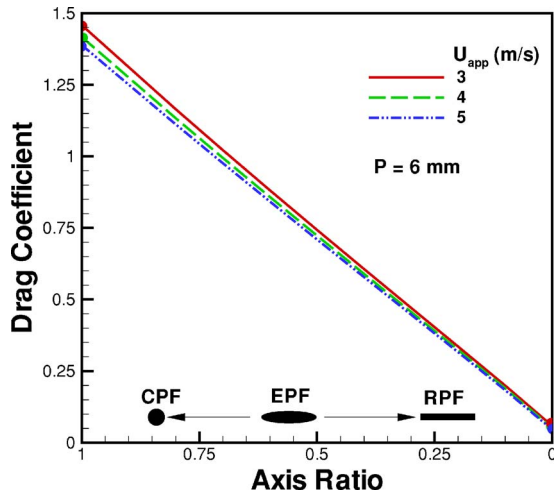


Fig. 6 Effect of the axis ratio on drag coefficients

The comparison of the overall performance of the selected geometries, on the basis of dimensionless entropy generation rate, is shown in Figs. 8–11 for the same perimeter. Figure 8 shows the variation of dimensionless entropy generation rate,  $N_s$ , with the Reynolds number, for the selected geometries. All the other parameters are kept constant. As the Reynolds number increases, the optimum dimensionless entropy generation rate decreases from SPF to RPF. The square pin-fin (SPF) gives the highest optimum entropy generation rate, whereas RPF gives the lowest optimum. It should be noted that each geometry has its own optimum for  $N_s$  which gives an optimal Reynolds number  $Re_{\mathcal{L}_{opt}}$  that increases also from SPF to RPF. Thus CPF and EPF with smaller axis ratios give best performance for lower Reynolds numbers, whereas RPF gives better performance for higher Reynolds numbers. For EPF with different axis ratios, the dimensionless entropy generation rate versus Reynolds number is shown in Fig. 9. It shows that the optimum dimensionless entropy generation rate decreases with the axis ratio and increases with the increase in Reynolds number. As a result, the overall performance increases with the increase in Reynolds number and decrease in axis ratio.

The effects of the aspect ratio on the dimensionless entropy generation rate for different geometries is shown in Fig. 10. Again, each geometry has its own optimum point for the minimum entropy generation rate which moves down towards lower

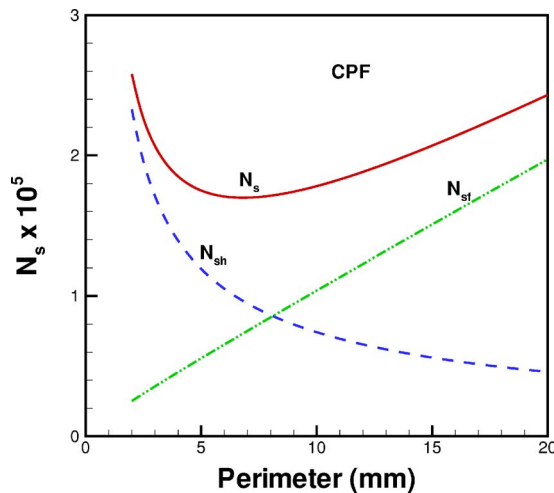


Fig. 7 Contribution of heat transfer and friction irreversibilities in dimensionless entropy generation rate

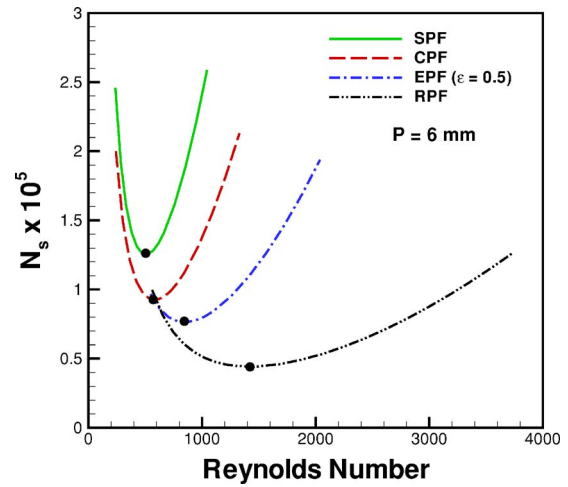


Fig. 8 Dimensionless entropy generation rate versus Reynolds number for different geometries

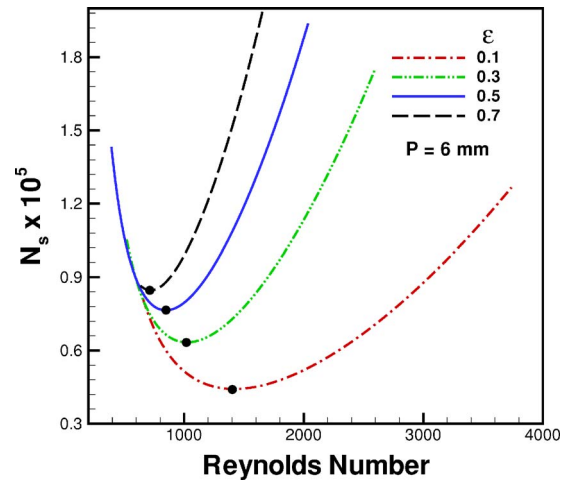


Fig. 9 Dimensionless entropy generation rate versus Reynolds number for elliptical geometry

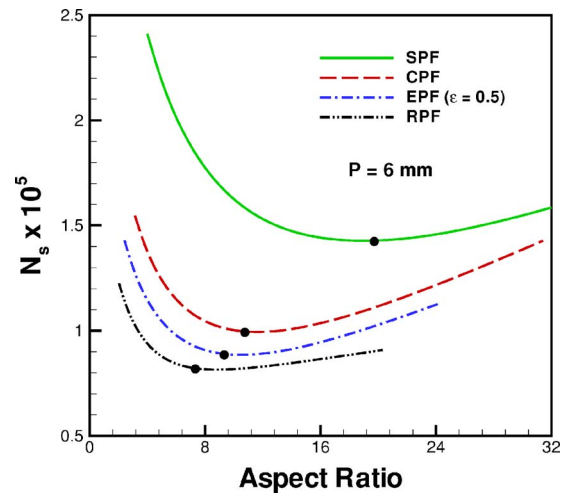
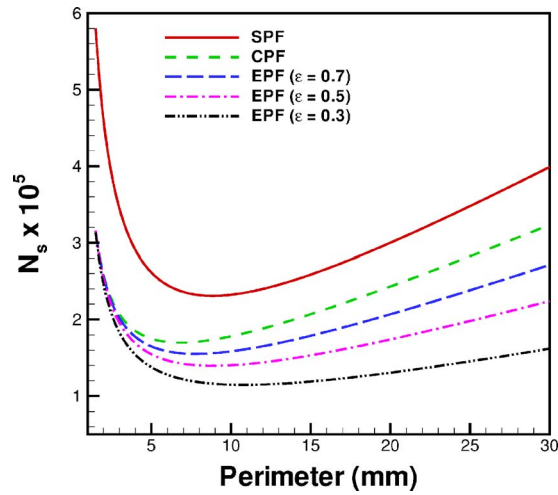


Fig. 10 Effect of aspect ratio on dimensionless entropy generation rate



**Fig. 11 Effect of perimeter on dimensionless entropy generation rate**

aspect ratio from the square geometry to the plate fin. Thus optimum aspect ratio is the highest for the SPF and lowest for RPF and hence RPF with smaller aspect ratios gives the best overall performance.

The effect of the perimeter on the dimensionless entropy generation rate, for all geometries, is shown in Fig. 11. Again the SPF gives the highest optimum dimensionless entropy generation rate. The optimum dimensionless entropy generation rate  $(N_s)_{opt}$  decreases with the increase in perimeter from SPF to RPF. Thus RPF will give the best performance for larger perimeters, whereas for smaller perimeters, CPF and EPF with smaller axis ratios will perform better.

## Conclusions

Different fin geometries having the same perimeter are compared from the point of views of heat transfer, drag force, and dimensionless total entropy generation rate. Optimum dimensionless entropy generation rate exists for each geometry corresponding to Reynolds number, perimeter, axis ratio in case of EPF, and the aspect ratio. The square geometry is found to be the worst choice from the point of view of heat transfer and drag force and hence from the point of view of total entropy generation rate. Whereas, the circular geometry performs better from the point of view of the dimensionless total entropy generation rate for smaller perimeters, larger aspect ratios and lower Reynolds numbers. The RPF gives the best results from the point of view of total entropy generation rate for higher Reynolds numbers, smaller aspect ratios and large perimeters. The elliptical geometry is the next most favorable geometry from the point of view of total entropy generation rate for higher Reynolds numbers and with smaller axis ratios. It offers higher heat transfer coefficients and lower drag force as the axis ratio is decreased and the approach velocity is increased.

## Acknowledgment

The authors gratefully acknowledge the financial support of the Center for Microelectronics Assembly and Packaging and Natural Sciences and Engineering Research Council of Canada.

## Nomenclature

- $A_c$  = cross sectional area of the fin [m<sup>2</sup>]
- $A_p$  = planform area for drag force [m<sup>2</sup>]
- $a, b$  = semi major and minor axes of the elliptical fin [m]
- $B$  = duty parameter  $\equiv \rho v^3 k T_a / Q^2$

- $C_D$  = total drag coefficient
- CPF = circular pin fin
- $c_p$  = specific heat of the fluid [J/kgK]
- $D$  = pin diameter [m]
- EPF = elliptical pin fin
- $E(e)$  = complete elliptic integral of second kind
- $e$  = eccentricity in case of elliptical geometry  $\equiv \sqrt{1 - \epsilon^2}$
- $F_D$  = drag force [N]
- $H$  = fin height [m]
- $k$  = thermal conductivity [W/mK]
- $k_{eq}$  = ratio of thermal conductivity of fluid to the fin material  $\equiv k_f / k$
- $h$  = average heat transfer coefficient [W/m<sup>2</sup> K]
- $L$  = length of baseplate in flow direction [m]
- $l$  = length of plate fin [m]
- $\mathcal{L}$  = characteristic length of fin [m]
- $m$  = fin performance parameter [m<sup>-1</sup>]
- $\dot{m}$  = mass flow rate [kg/s]
- $N_s$  = total dimensionless total entropy generation rate
- $N_{sf}$  = fluid flow irreversibility
- $N_{sh}$  = heat transfer irreversibility
- $Nu_{\mathcal{L}}$  = Nusselt number based on the characteristic length of the fin  $\equiv h\mathcal{L} / k_f$
- $P$  = perimeter of the fin [m]
- Pr = Prandtl number
- $Q$  = total base heat flow rate [W]
- RPF = rectangular plate fin
- $Re_{\mathcal{L}}$  = Reynolds number based on the characteristic length of the fin  $\equiv U_{app}\mathcal{L} / \nu$
- $R_{tot}$  = total thermal resistance [K/W]
- $\dot{S}_{gen}$  = total entropy generation rate [W/K]
- SPF = square pin fin
- $s$  = side of a square fin [m]
- $T$  = temperature [K]
- $t$  = thickness [m]
- $U_{app}$  = approach velocity of the fluid [m/s]
- $W$  = width of baseplate [m]
- $w$  = width of plate fin [m]

## Greek Symbols

- $\epsilon$  = axis ratio of elliptical fin  $\equiv b/a$
- $\epsilon_1$  = ratio of the plate sides  $\equiv t/L$
- $\gamma$  = aspect ratio  $\equiv H/\mathcal{L}$
- $\nu$  = kinematic viscosity of fluid [m<sup>2</sup>/s]
- $\rho$  = fluid density [kg/m<sup>3</sup>]

## Subscripts

- $a$  = ambient
- $b$  = baseplate
- $f$  = fluid
- $w$  = wall

## References

- [1] Behnia, M., Copeland, D., and Soodphadakee, D., 1998, "A Comparison of Heat Sink Geometries for Laminar Forced Convection," *Proceedings of The Sixth Intersociety Conference on Thermal and Thermomechanical Phenomena in Electronic Systems*, Seattle, Washington, USA, May 27–30, pp. 310–315.
- [2] Li, Q., Chen, Z., Flechtner, U., and Warnecke, H. J., 1998, "Heat Transfer and Pressure Drop Characteristics in Rectangular Channels With Elliptical Pin Fins," *Int. J. Heat Fluid Flow*, **19**, pp. 245–250.
- [3] Chapman, C. L., Lee, S., and Schmidt, B. L., 1994, "Thermal Performance of an Elliptical Pin Fin Heat Sink," *Proceedings of the Tenth IEEE Semi-Therm Symposium*, pp. 24–31.
- [4] Ota, T., Aiba, S., Tsuruta, T., and Kaga, M., 1983, "Forced Convection Heat Transfer From an Elliptical Cylinder," *Bull. JSME*, **26**(212), pp. 262–267.
- [5] Ota, T., Nishiyama, H., and Taoka, Y., 1984, "Heat Transfer and Flow Around an Elliptical Cylinder," *Int. J. Heat Mass Transfer*, **27**(10), pp. 1771–1779.
- [6] Poulikakos, A., and Bejan, A., 1982, "Fin Geometry for Minimum Entropy Generation in Forced Convection," *J. Heat Transfer*, **104**, pp. 616–623.

- [7] Jonsson, H., and Bjorn, P., 1996, "Experimental Comparison of Different Heat Sink Designs for Cooling of Electronics," *ASME J. Heat Transfer*, **329**(7), pp. 27–34.
- [8] Wirtz, R. A., Sohal, R., and Wang, H., 1997, "Thermal Performance of Pin-Fin Fan-Sink Assemblies," *J. Electron. Packag.*, **119**, pp. 26–31.
- [9] Laor, K., and Kalman, H., 1992, "Performance and Temperature Distributions in Different Fins With Uniform and Nonuniform Heat Generation," *Inst. Chem. Eng. Symp. Ser.*, **1**(129), pp. 335–342.
- [10] Mokheimer, E., M. A., 2002, "Performance of Annular Fins With Different Profiles Subject to Variable Heat Transfer Coefficient," *Int. J. Heat Mass Transfer*, **45**(17), pp. 3631–3642.
- [11] Culham, J. R., and Muzychka, Y. S., 2001, "Optimization of Plate Fin Heat Sinks Using Entropy Generation Minimization," *IEEE Trans. Compon. Packag. Technol.*, **24**(2), pp. 159–165.
- [12] Bar-Cohen, A., and Iyengar, M., 2003, "Least-Energy Optimization of Air-Cooled Heat Sinks for Sustainable Development," *IEEE Trans. Compon. Packag. Technol.*, **26**(1), pp. 16–25.
- [13] Iyengar, M., and Bar-Cohen, A., 2003, "Least-Energy Optimization of Forced Convection Plate-Fin Heat Sinks," *IEEE Trans. Compon. Packag. Technol.*, **26**(1), pp. 62–69.
- [14] Iyengar, M., and Bar-Cohen, A., 2001, "Design for Manufacturability of SISE Parallel Plate Forced Convection Heat Sinks," *IEEE Trans. Compon. Packag. Technol.*, **24**(2), pp. 150–157.
- [15] Bar-Cohen, A., Iyengar, M., and Kraus, A. D., 2003, "Design of Optimum Plate-Fin Natural Convective Heat Sinks," *ASME J. Electron. Packag.*, **125**(3), pp. 208–216.
- [16] Bejan, A., *Entropy Generation Minimization*, CRC Press, New York, 1996.
- [17] Khan, W. A., Culham, J. R., and Yovanovich, M. M., 2004, "Fluid Flow and Heat Transfer from Elliptical Cylinders," *J. Thermophys. Heat Transfer*, **19**(2), pp. 178–185.
- [18] Jakob, M., 1949, *Heat Transfer*, Wiley, New York, Vol. 1.